Effects of Rain Rate and Wind Magnitude on SeaWinds Scatterometer Wind Speed Errors

DAVID E. WEISSMAN

Hofstra University, Hempstead, New York

MARK A. BOURASSA

COAPS/The Florida State University, Tallahassee, Florida

JEFFREY TONGUE

National Weather Service, Upton, New York

(Manuscript received 9 October 2000, in final form 10 October 2001)

ABSTRACT

Rain within the footprint of the SeaWinds scatterometer on the QuikSCAT satellite causes more significant errors than existed with its predecessor, the NASA scatterometer (NSCAT) on *Advanced Earth Observing Satellite-I* (*ADEOS-I*). Empirical relations are developed that show how the rain-induced errors in the scatterometer wind magnitude depend on both the rain rate and on the wind magnitude. These relations are developed with collocated National Data Buoy Center (NDBC) buoy measurements (to provide accurate sea surface winds) and simultaneous Next Generation Weather Radar (NEXRAD) observations of rain reflectivity. An analysis, based on electromagnetic scattering theory, interprets the dependence of the scatterometer wind errors on volumetric rain rate over a range of wind and rain conditions. These results demonstrate that the satellite scatterometer responds to rain in a manner similar to that of meteorological radars, with a Z–R relationship. These observations and results indicate that the combined (wind and rain) normalized radar cross section will lead to erroneously large wind estimates when the rain-related radar cross section exceeds a particular level that depends on the rain rate and surface wind speed.

1. Introduction

Scatterometers are microwave radars that use the intensity of signals that are returned from the wind-roughened surface to estimate wind speed and direction over the ocean. The wavelength and incidence angles (>45°) of the scatterometer's microwaves is such that they are primarily backscattered by centimeter-sized ripples (capillary waves). The density and size distribution of ripples responds very quickly to changes in winds and has relatively little sensitivity to larger waves, making it very practical for determining surface winds and wind stress. While the scatterometer can easily penetrate clouds without interference, rainfall interferes with the capability to estimate sea surface winds because it affects the small-scale surface roughness, the attenuation, and scattering of the radar signal in the atmosphere.

Scatterometers have the potential to observe and measure coastal storm conditions. This data can supplement the resources available to the National Weather Service (NWS) for their coastal watch and warning activities. However, the presence of rain has been seen to introduce errors into the nominal SeaWinds scatterometer wind products. This is true for any area of the ocean. This research effort seeks to quantify the interfering effects of rain on these wind estimates. The near-continuous observations of the Next Generation Weather Radar (NEXRAD) stations near the coastlines and buoys provide the coincident dataset needed for these studies. This concurrent situation provides a near-ideal field laboratory for empirical and physical studies. It is intended that the results assist in the interpretation of scatterometer data, especially for near-real-time applications. It is yet to be determined whether this assistance will involve corrections to wind products or to the identification ("rain flagging") and discarding of affected data. Our physical studies of the electromagnetic backscatter from rain, to be presented here, provide guidance about the relative magnitude of the radar cross section of the rain relative to that from the sea surface. Passive satellite sensors, microwave radiometers such as the special sen-

Corresponding author address: Dr. David E. Weissman, Department of Engineering, Hofstra University, 104 Weed Hall, Hempstead, NY 11549.
E-mail: eggdew@hofstra.edu

sor microwave imager (SSM/I) (Wentz 1997), may estimate sea surface winds with acceptable spatial resolution but are severely affected by clouds and are ineffective when rain is present.

The SeaWinds scatterometer on the QuikSCAT mission (QSCAT) was launched in June 1999. Its development was a rapid response to the unfortunate loss of the *Advanced Earth Observing Satellite-I* (*ADEOS-I*) spacecraft in June 1997: *ADEOS-I* carried the National Aeronautics and Space Administration (NASA) scatterometer (NSCAT) and several other instruments. The single swath of the SeaWinds radar has a width of 1800 km, with wind vector estimates averaged over each 25 $\times$ 25 km^2 area within it. Surface locations are illuminated an average of ~2 times each day. SeaWinds' function is to measure global sea surface winds, with the intention of providing this data to the meteorological and oceanographic scientific communities, as well as the general research community.

When rain is not present, current evidence indicates that SeaWinds provides, overall, a more accurate wind vector product than NSCAT (Bourassa et al. 2002, hereafter BLOS; Ebuchi 2001). Considering what has been learned about model function development since NSCAT, this is to be expected. The Geophysical Model Function is the algorithm used to extract wind vector estimates from the assembly of normalized radar cross-section (NRCS) measurements acquired by the multiple beams. It is continually under vigorous development so that further improvements can be expected in the future (JPL 2001). Comparisons with buoys indicate that rms differences in speed are <1 m s^{-1} in the absence of rain; and comparisons to research vessels indicate uncertainties in speed of <0.5 m s^{-1} (BLOS). Buoy winds are generally accepted to have an accuracy of 1 m s^{-1} or 10%, whichever is larger.

The SeaWinds radar operates at a frequency of 13.4 GHz. The antenna system creates a different viewing geometry than was the case for NSCAT. Instead of the fixed angle fan beams used by NSCAT, which collected signals from a range of incidence angles, from 18° to 59°, this instrument uses a rotating dish antenna with two spot beams that sweep in a circular patterns, and receives horizontal polarization (H-Pol) at 46.25° and vertical polarization (V-Pol) at 54°. For reasons to be discussed below, this new antenna illumination provides a condition whereby rain causes greater errors in the scatterometer wind estimates. The transmitter emits pulses sufficiently long to create an effective continuous wave (CW) radar, which measures the average radar cross section of a specific area of the sea surface (the NRCS). The common symbol for this quantity is σ^0. The microwaves scatter off of ripples, which respond very quickly to changes in wind speed.

The influences on the backscattered signal due to rain are attenuation, rain volume backscatter (Moore et al. 1979), and changes in sea surface roughness (Craeye et al. 1997), all of which introduce errors into the process of estimating surface winds. When rain strikes the water surface the shape is modified. Rain impact causes ripples as well as crowns and stalks, each of which interact with the radar's microwaves.

Rain modifies the signal received by the radar, resulting in the wind vector estimates having greater error than rain-free cases. This issue is more important for QSCAT than it was for NSCAT because the NRCS higher incidence angles are more strongly affected by raindrops and the rain-roughened surface. Evidence for this is sparse, but airborne measurements at 10 GHz during the Tropical Ocean Global Atmosphere Coupled Ocean–Atmosphere Response Experiment (TOGA COARE) (Craeye 1998) provide useful data. For example, when the wind speed is 6 m s^{-1}, a rain rate of 5.5 mm h^{-1} will cause the V-Pol radar cross section to increase by 2 dB at an incidence angle of 35°. However if the incidence angle is 50°, the radar cross section will increase by 7 dB for this rain rate. In the NSCAT configuration, about one-half of the wind vector cells were measured at an incidence angle less than 40°. Therefore, on a swath-averaged basis, the problem of rain-induced errors is a more serious issue for QSCAT than it was for NSCAT. The fact that these errors occur, combined with results presented herein, indicates additional needs for future research. At the current time, methods are being developed for detecting the presence of signal contamination due to rain: these techniques produce "rain-flags" (Mears et al. 2000; Huddleston and Stiles 2000), and "quality indicators" (Portabella and Stoffelen 2001). The results to be presented here provide quantitative information about the size of the wind magnitude estimation errors that can occur.

2. NEXRAD properties and data

The NEXRAD network (operated by the NWS) spans the entire United States with over 160 stations. These S-band instruments [designated Weather Surveillance Radar-1988 Doppler (WSR-88D)] provide sensitive, fine-resolution precipitation observations every 5–10 min. They operate at frequencies in the range 2.7–2.9 GHz. NEXRAD systems provide measurements of radar reflectivity, spectrum width, and wind radial velocity. They generate up to 39 categories of analysis products derived from the base data. These can involve hydrometeorological algorithms and combinations of spatial resolution and coverages (Klazura and Imy 1993). On the East Coast, there are about 10 stations between Florida and Massachusetts that enable measurements coincident with the QSCAT swath. Almost all of these NEXRAD sites have at least one National Data Buoy Center (NDBC) buoy within its range. These buoys can provide a wind estimate for comparison with QSCAT estimates.

The antenna, with a beamwidth of 0.95°, continuously monitors its environment on a preprogrammed sequence of 360° azimuth sweeps at various incidence angles, from 0.5° to 19.5° (precipitation mode). Two WSR-88D

Level III data products are used in this study. One is the base reflectivity product from the 0.5° elevation scan. This product is stored in polar coordinates, with 16 levels of reflectivity in steps of 5 dBZ. It is converted into a rectangular grid in our data analysis. The other data product, composite reflectivity, is a "volume" product. It uses reflectivity from all radar elevation levels that constitute the conical volume. Each data element in the resulting gridded product contains the maximum reflectivity observed by the radar at a particular location, regardless of elevation. Therefore, adjacent grid boxes in the display may contain reflectivity values from different elevation scans. The product contains no information about the height or vertical extent of the rain column at that location. The specific products selected for this study have a horizontal resolution of 4 km. When rain rate was estimated in our analysis, the Z–R relation we adopted was that commonly used in WSR-88D algorithms: $Z = 300\ R^{1.4}$ (Hunter 1996). Brightband contamination, which is enhanced reflectivity due to melting of frozen precipitation aloft, can occur near or just below the freezing level. The brightband nominal height in the climatological summer is at an average of 4 km. The brightband spatial extent may be on the same scale as the scatterometer cells (Schumacher and Houze 2000). If that is taking place, the NEXRAD may infer an excessive amount of reflectivity, but on balance the scatterometer will also infer a proportionately higher backscatter due to reflections from the bright band.

Some blockage of the beam exists (increasing with range) because of earth curvature and standard refraction. This means that the full vertical rain column can not be observed. At a range of 100 km, the beam can receive backscatter from the altitude range 800–5000 m (Hunter 1996). These height quantities are approximate proportional to range. It is possible that, at the higher ranges, a highly inhomogeneous vertical profile may lead to errors in the recorded estimate.

The accuracy of the WSR-88D radars in estimating rainfall can be viewed as three separate issues. One is the Z–R formula that can best match the specific meteorological conditions for a given observation. Battan (1973) lists a large number of published Z–R relationships, for specific rain conditions and geography. This diversity illustrates the nature of the problem. Rain events (and local drop-size distributions) are too variable to support the expectation that a single Z–R formula has the same accuracy in all situations. However, for the purpose of this present study, we believe that the one selected above is a reasonable assumption for the datasets that are currently available. The second issue relating to accuracy is that of the radar calibration and how this affects the estimate of Z. The potential errors related to the present method of WSR-88D calibration are thoroughly discussed by Ulbrich and Lee (1999). Using surface measurements for comparison, they suggest that the calibration measurement of a critical constant used in the radar equation may be a cause of some errors. They point out that rainfall estimates could be in error by a factor of 2 as a result of current practice for the WSR-88D. The ramifications and resolution of their concerns needs time for further exploration. The third consideration is that the NEXRAD data products we use are quantized in 5-dBZ increments. This resolution issue dominates the uncertainty in our SeaWinds/NEXRAD/buoy data analysis, and the second consideration dominates biases in rain rate. The step in Z of 5 dB corresponds to a factor 2.3 in rain rate using the algorithm cited above.

3. Coincident rain, buoy, and QSCAT measurements

The virtually instantaneous collocation of NEXRAD rain measurements with QuikSCAT and buoy observations is an important advance in the quantitative determination of the effect of rainfall on QuikSCAT wind estimates. The NEXRAD data products consist of radar scans taken only 6 min apart, so that the temporal coincidences with QSCAT observations are sufficiently close to be viewed as effectively instantaneous. Considering how rapidly rain cell spatial structures evolve and how rain intensity varies with time, this close a time difference is essential in order to have a valid observation of what is affecting the QSCAT measurement. The buoys and NEXRAD sites that could be used in this study were found by applying two constraints. The first consideration was that the buoys and NEXRAD sites had to be within 150 km of each other. The second constraint was that the buoy had to be sufficiently far (~25 km) from land and that the scatterometer land mask (which extends ~30 km from the shoreline) did not prevent close collocations between scatterometer and buoy observations. All scatterometer observations within 150 km of the buoy, at the time of the selected overpass, were selected for this study. The preceding and following buoy observations (recorded at hourly intervals by the NDBC) were also extracted for this comparison. These two wind values were then interpolated to the time of the overpass. We are interested in the variability of wind averaged over the sampling volume of the scatterometer (~25 × 25 km^2). In the absence or rain, fronts, and orographic modification (by mountains), scatterometer wind fields are usually uniform over scales of several hundred kilometers. Examples can be found on the Center for Ocean–Atmospheric Prediction Studies (COAPS) scatterometry Web page (http://www.coaps.fsu.edu). In the examples discussed in this paper there are no fronts or orographic modification by mountains.

In order to assess the relative accuracy between QSCAT winds and the specific buoys used in this study, a graph was produced that plotted QSCAT winds versus buoy winds for all collocations over a 4-month interval. Scatterometer wind estimates were used only if the cell location was within 100 km of the buoy. Over 4000 data

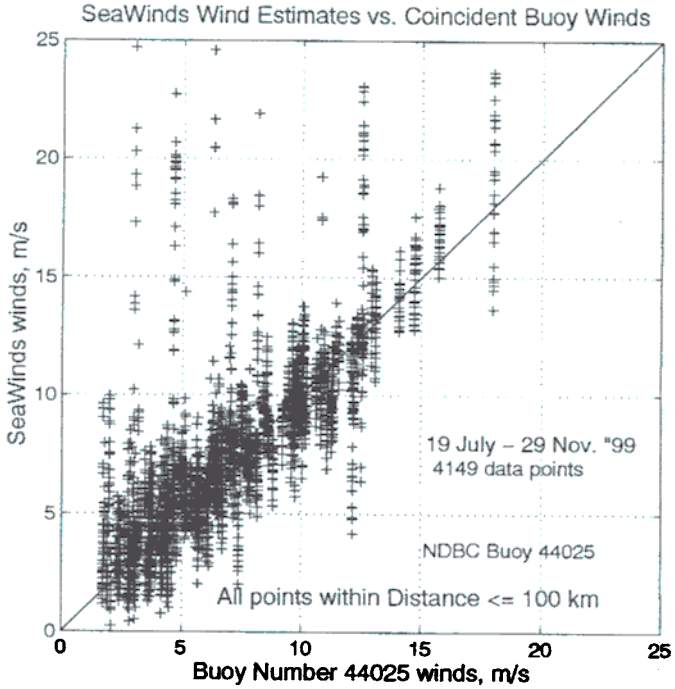

FIG. 1. Scatterometer estimates of sea surface winds in the vicinity of buoy 44025, off the coast of Long Island, New York, for a 10-week interval. The wind magnitudes (Level 2B data) are collected from cells within 100 km of the buoy and plotted vs the buoy wind estimate (corrected for neutral stability) computed by interpolating the QSCAT orbit time between the hourly buoy samples. The scatterometer wind magnitude accuracy has been determined to be less than 1 m s^{-1}, and the buoy wind accuracy 1 m s^{-1} or 10%, whichever is larger.

points were collected, and are plotted in Fig. 1. It should be noted that one buoy data point is associated with several scatterometer wind estimates. For the great majority of observations, the relative agreement is seen to be very good and within the combined uncertainties of both sensors and the small-scale variability to which the buoy is sensitive. For seven or eight collocations we detect anomalous excursions of the QSCAT wind. In most of these cases very large scatterometer wind speeds were estimated. The common 0.3–1.2 m s^{-1} differences between buoy (or ship) winds and scatterometer winds (Bourassa et al. 1997; BLOS; Freilich and Dunbar 1999) under clear conditions were found to be small in comparison to the errors hypothesized to be caused by rain within the scatterometer field of view. We believe that these excessive wind estimates are evidence of appreciable rainfall within the scatterometer beam. This interpretation will be supported by our collocation analysis and theoretical electromagnetic analysis.

The assessment of rain influences on scatterometer wind speeds through the use of NEXRAD-based estimates of rain rate within the radar resolution volume is addressed through three considerations. One is to note the properties of the physical variability (dynamic meteorological processes) that cause variations within this spatial volume. SeaWinds/buoy mismatches due to this consideration are referred to as measurement errors. The second consideration is the sensitivity of the QSCAT wind estimates to rain, including determination of the dynamic range of rain rate that is significant. The instrument errors inherent in the WSR-88D must also be considered. Regarding QSCAT sensitivity, the measured results indicated that rain events are characterized by a range of several decades in rain rate (R), and errors of a factor of 2 in rain rate are not observed to cause significant errors in QSCAT interpretations. This is especially important because the spatial distribution of the rain within the 25 km × 37 km surface ellipse used to approximate the scatterometer footprint (JPL 2001, section 5.2.2) will usually not be homogenous. This problem is usually referred to as nonuniform beam filling and is known to be a source of error (Durden et al. 1998). As with all antenna illumination definitions, some energy may be received from areas just outside this boundary; however, this energy has reduced amplitude as determined by the antenna pattern shape. In addressing the spatial and temporal variability of the rain structures, we have selected a 28 km × 28 km bin average in the algorithms used to estimate the rain rate. This numerical value is then used in our subsequent discussions of "rain rate." This simplification of the rain description is justified through the fact that the backscattered signal at the satellite will be an "average," which is more difficult to define precisely. The SeaWinds NRCS is affected by the three-dimensional nature of the volume scattering, the atmospheric attenuation, and the additional effect of surface roughness perturbations, which can vary across the footprint. Based on the information we have, higher spatial resolution of the rain is not justified. The common 0.3–1.2 m s^{-1} error differences between buoy (or ship) winds and QSCAT winds (Bourassa et al. 1997; BLOS; Freilich and Dunbar 1999) under clear conditions were found to be small in comparison to the errors caused by rain within the scatterometer field of view.

A NEXRAD Level III "composite reflectivity" data product with 4-km spatial resolution is shown in Fig. 2. The rain rate is displayed as a quantized color scale for the reflectivity factor, Z, in 5-dBZ steps. The concentric circles are centered at the NEXRAD site and represent range steps of 115 km. The latitude and longitude lines are 1° each. The Long Island and New Jersey coastlines are discernible. The location of buoy 44025 is represented in Fig. 2 by a star; it serves as the approximate center of the QSCAT dataset (from the Level 2B data archive provided by the project). It is approximately 80 km from the NEXRAD. Considerable spatial variability, with large changes in rain rate (30 dBZ in a few kilometers) is characteristic of rain events. Only those "wind vector cells" (WVC) within 150 km of the buoy are collected in this study. Since the QSCAT resolution for a wind cell is approximately a 25-km square, appreciable averaging of the NEXRAD resolution elements will be necessary to create an equivalent spatial rain estimate. While this averaging will be a

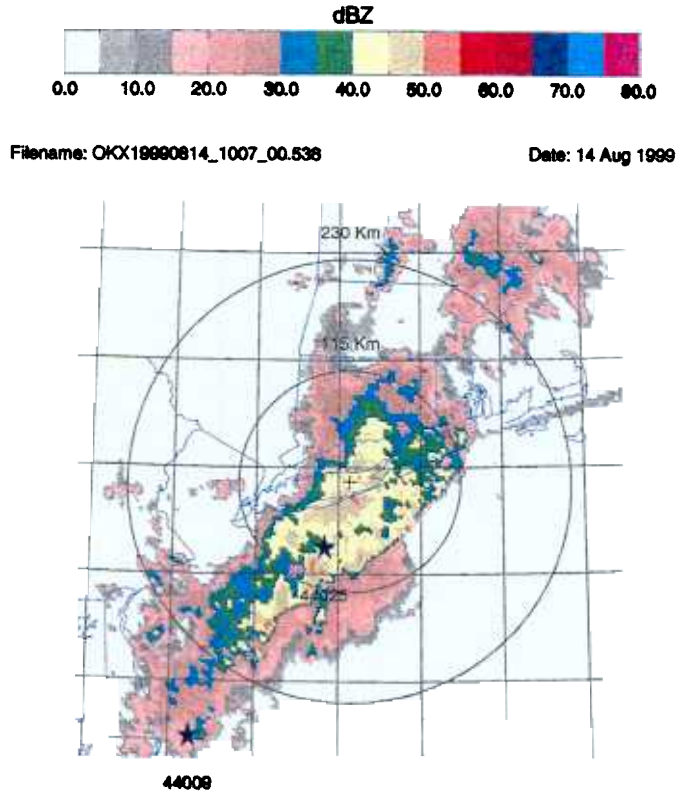

FIG. 2. Geographical representation of the magnitude of the composite reflectivity (quantized in 16 discrete levels of 5 dBZ) derived from a 6-min scan of the WSR-88D. This was observed by the NEXRAD radar station of the NWS office at the Brookhaven National Laboratory, on 14 Aug 1999. Buoys 44009 and 44025 are indicated at their geographic locations with stars. The grid spacing is 1°.

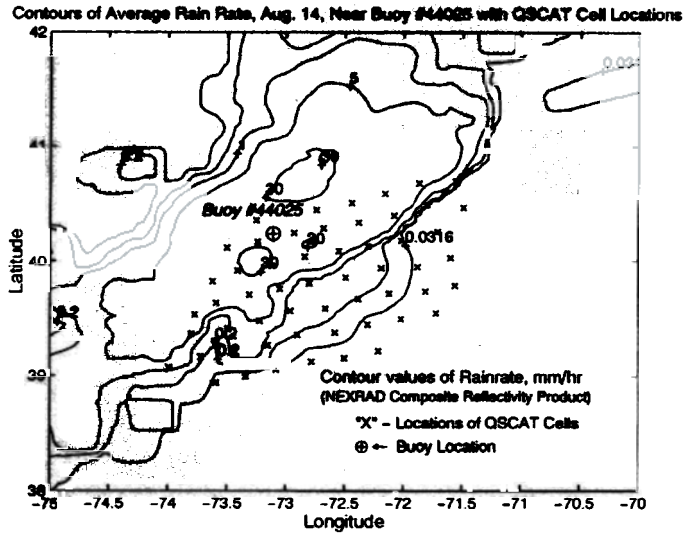

FIG. 3. Conversion of rain intensities of NEXRAD data in Fig. 2. from dBZ into rain rate on a 4-km grid; each point is an average over a 28 × 28 km² area. The contour lines (mm h^{-1}) reflect the rain-rate levels in and near their respective paths. The "x" values are at the centers of the 25-km QSCAT wind vector cells. Differences between the QSCAT wind magnitude and the buoy wind speed can be compared with the rain rate at each "x," graphically approximated by the contours.

linear operation on a single two-dimensional variable (mean of a 7 × 7 array of 4-km elements), it is not likely that the QSCAT's backscattered NRCS, which combines both the sea surface reflections, the atmospheric attenuation, and volume scattering, can be viewed as a linear combination or average. The quantization of NEXRAD's Z into 5-dBZ steps leads to the well-known quantization noise that limits the precision of the rain-rate estimates. If each 4-km NEXRAD cell is assigned a noise value (i.e., uncertainty) based on its absolute level and this quantization increment, then these uncertainties for each rain-rate estimate can be summed in the mean-square to produce a root-mean-square level for the full 28 km × 28 km array. The total uncertainty estimate will depend on the range of rain rates with the 28 × 28 km² area. This uncertainty is used as error bars for plots involving these mean NEXRAD rain-rate estimates.

An example of the benefits of this collocated dataset is seen when the data collected on 14 Aug 1999 (Fig. 2) is analyzed. This event took place at 1007 UTC. The rain conditions are the typical, highly variable rain intensities. This rectangular image extracted from this NEXRAD data file is then filtered using spatial averages. The numerical value of each array element is transformed from the 4-km radar reflectivity (after conversion from dBZ to linear Z units, and then to rain rate) to a mean of the rain-rate values of the 7 × 7 array (a 28 km × 28 km area) centered at each original point. This represents a 28 km × 28 km area. This is done so that each QSCAT estimate of the wind vector, based on the typically 8–20 NRCS measurements within this area, can be compared to a "rain rate" that represents an average over the same sized area. In addition to matching it to the QSCAT cell size, this tends to compensate for possible errors in NEXRAD cell locations and Z values (Hunter 1996).

The method selected for displaying the two-dimensional distribution of the mean rain rates is the contour diagram. The shapes of rain-rate contour lines (Fig. 3) resemble the borders of the constant-color regions seen in Fig. 2. The rain-rate contours have values of 0.03, 0.2, 5.0, and 30 mm h^{-1}, and the buoy location is identified with a special symbol. Those QSCAT cells within the swath that lie within the distance limit mentioned above (within 150 km of the buoy) are labeled with an "x." The QSCAT cells are distributed within either high-, low-, or no-rain regions. The striking benefit of this approach is that we can easily observe a wide dynamic range of rain intensities throughout a QSCAT swath, for a relatively uniform wind condition. It is analogous to having a "laboratory" in which it is possible to vary one of the key independent variables. The difference between the QSCAT wind magnitudes at each point ("x") and the buoy wind (4.6 m s^{-1}) is then plotted in Fig. 4. A clear functional dependence and monotonic trend is displayed. Several features of this figure deserve discussion; however, the principal ob-

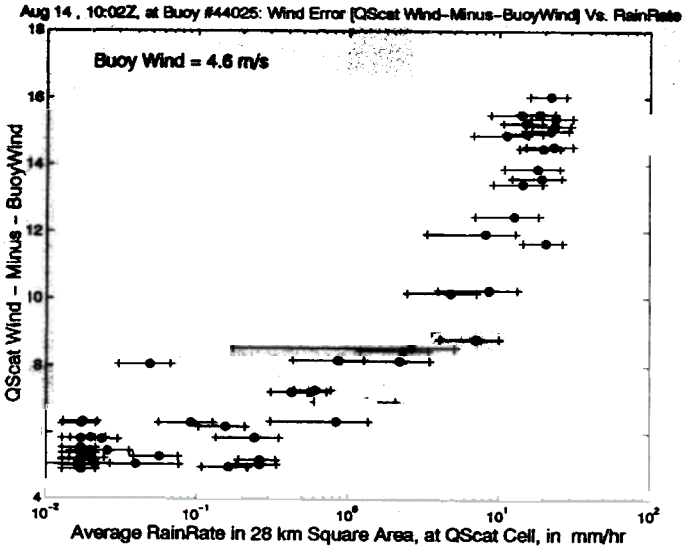

FIG. 4. The difference (QSCAT error) between the QSCAT wind magnitude and buoy wind magnitude (m s^{-1}) as a function of rain rate at the location of the QSCAT wind vector cell (see Fig. 3). A very clear, monotonic relationship is observed, on average. The buoy wind speed, interpolated between its hourly readings for the QSCAT time, was 4.6 m s^{-1}.

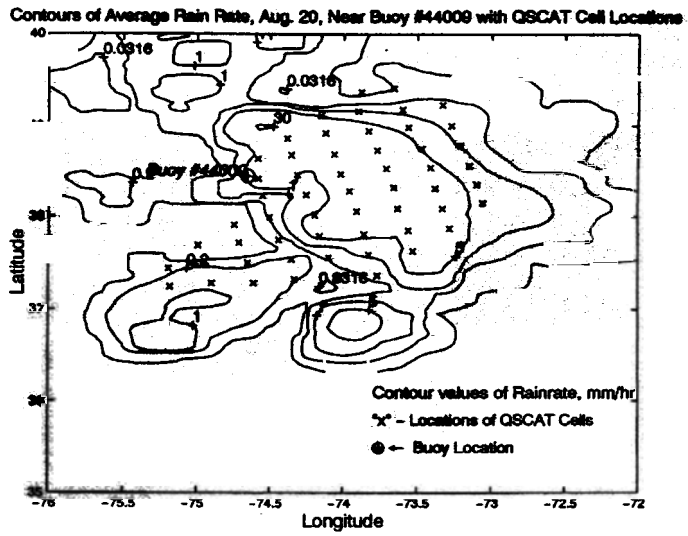

FIG. 5. Conversion of rain intensities of NEXRAD data in taken on 20 Aug 1999, near buoy 44009, from dBZ into rain rate on a 4-km grid; each point is an average over a 28 × 28 km^2 area. The contour lines reflect the rain-rate levels in and near their respective paths. The "x" values are at the centers of the 25-km QSCAT wind vector cells. Differences between the QSCAT wind magnitude and the buoy wind speed can be compared with the rain rate at each "x," graphically approximated by the contours (mm h^{-1}).

servation is that above a rain rate of 1 mm h^{-1}, the wind speed error increases with a substantial slope. Even at lower rain rates, the magnitude of the errors compared to the buoy wind speed is very significant. This group of results is impressively self-consistent with respect to the relatively small scatter in these errors, considering the highly complex processes involved. No negative differences were observed in this particular event, but they were in other cases (see Fig. 6). These types of comparisons are always limited by the fact that the buoy responds to a much smaller sampling volume than the scatterometer; therefore, even accurate measurements can differ substantially from accurate scatterometer measurements. In this case, the buoy is probably underestimating the winds sampled by the scatterometer.

An apparent anomaly is seen in Fig. 4, where the difference between QSCAT wind and buoy wind is seen to be large, greater than 5 m s^{-1}, even though the NEXRAD rain rate is less than 0.3 mm h^{-1}. A possible explanation is that there existed a higher rain rate at these scatterometer cell locations than was detected by the NEXRAD system. This could be due to some type of limitation in the NEXRAD data-acquisition technique, propagation condition of the atmosphere, or related error mechanism. Many of these "low rain-rate" cells occurred at a substantial distance from the NEXRAD site (>100 km) (see Figs. 2 and 3), where its beam will not illuminate much of the atmosphere below 1000 m. If there was appreciable rain in this lower-altitude region, it would create higher σ^0 but an insufficient population of large NEXRAD Z values. Another possible condition may be that only the NEXRAD cannot accurately measure the rain rate at the top of the rainfall column. Since we are using the composite reflectivity data, the highest Z levels that it captures may still be less than what was in the rain column. An undetected presence of 0.5 mm h^{-1} averaged rain would explain the observed anomaly. This could imply a relatively larger scatterometer radar cross section, relative to the nonrain observations. If rain volume backscatter is the dominant mechanism, this would explain the apparently higher wind speeds. Alternatively, there could be greater wind speeds due to spatial inhomogeneities (i.e., a gust front). Unfortunately, no additional measurements are available to support any of these hypotheses.

The other NEXRAD product considered herein, the base reflectivity, is limited to the lowest elevation of this storm. Acquired at the same time as the data used in Fig. 2, the base reflectivity image was also examined. It was found to display lower levels of reflectivity where the composite reflectivity found high rain areas. It showed no rain both more than 50 km southeast of the buoy and in other areas where Fig. 2 does show appreciable rain. This product would miss the rain that would exist at the higher altitude and with which the scatterometer would interact. Figure 3 shows a rain rate of about 1 mm h^{-1} starting at 50 km away from the buoy in the southeasterly direction, and extending for about another 75 km before it decreases. These would be missed by the base reflectivity product.

It is useful to examine similar relationships on another day with a higher wind speed, at a different location, as seen in the rain contour diagram of Fig. 5. These NEXRAD measurements, taken on 20 August 1999, were centered around buoy 44009, near Cape May, New Jersey. The maximum rain rate is about the same as that seen in Figs. 2 and 3, but there are more QSCAT cells

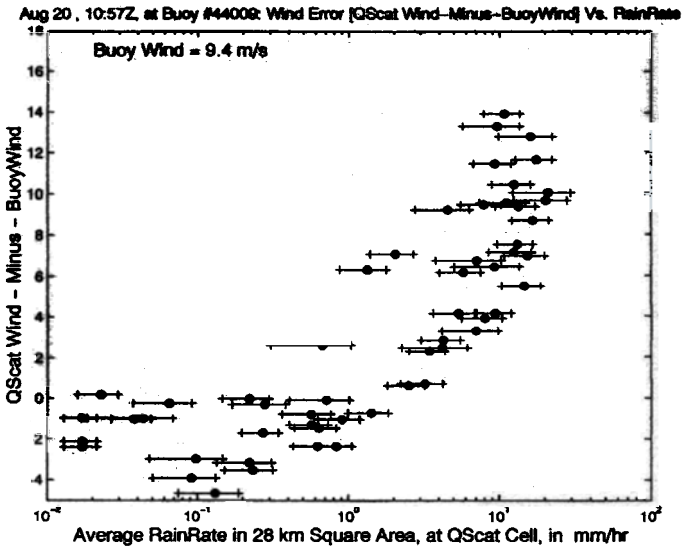

FIG. 6. The difference (QSCAT error) between the QSCAT wind magnitude and buoy wind magnitude (m s^{-1}) as a function of rain rate at the location of the QSCAT wind vector cell (see Fig. 5). A very clear, monotonic relationship is observed, on average. The buoy wind speed, interpolated between its hourly readings for the QSCAT time, was 9.4 m s^{-1}.

in the higher rain areas, in this collocation. The wind speed at this time was about 9 m s^{-1}. The differences between QSCAT wind and the buoy winds (Fig. 6), for rain rates less than 1 mm h^{-1}, show that most of the differences are within the QSCAT mission requirement limit of 2 m s^{-1}. As the rain rate increase beyond 3 mm h^{-1}, the size of the error exceeds this limit and grows rapidly to levels that make the QSCAT data ineffective for its intended purpose. Once the rain rate reaches the 15–20 mm h^{-1}, an interesting resemblance to the lower wind speed example appears; the scatterometer is producing wind estimates in the range of 19–23 m s^{-1}, for both of these surface wind speeds. This indicates that backscattered radar cross-section values are about the same for both wind speeds. This can be interpreted as representing total volumetric rain backscatter in the atmosphere, which would be independent of surface winds. This viewpoint will be discussed further in the next section.

4. Electromagnetic backscatter and radar issues

The important question of which electromagnetic scattering and propagation effect has the greatest influence on QSCAT wind estimates reduces to the three choices mentioned above: volume backscatter, path attenuation, or surface roughness due to rain impact. Attenuation reduces the radar cross section, so this can be eliminated as a cause of higher wind estimates. Rain impacting the surface may have a a relatively strong effect, once it passes an approximate threshold, but then the fractional increase in radar cross section tends to decrease (Craeye et al. 1997; Craeye 1998). Instead, Fig. 4 displays a steady increase, reflecting an almost proportional relationship. Therefore, rain-induced surface roughness will not be used as an interpretation of these results. There will likely be other circumstances (e.g., light winds and light rain) where the rain roughening will play a larger role.

The possibility that the large erroneous QSCAT wind values are the result of the increase in radar backscatter, due to the scattering from the volume of rain particles in the atmosphere will be examined analytically. The method is a one-dimensional formulation in which the principal terms are the volume backscattering coefficient, based on the electromagnetic interaction with individual spherical particles, combined with an attenuation term to model the diminishing amplitude of the wave as it penetrates a volume of this type. A rain-related SeaWinds backscatter model is developed, based on the Rayleigh approximation (Battan 1973), and the backscatter cross section of a spherical water particle at the frequency (13.4 GHz) of QuikSCAT (Ulaby et al. 1981). The result is related to the reflectivity factor, Z. The formula for the radar cross section per unit volume is

$$\sigma_{vr} = 10^{-10}\frac{\pi^5}{\lambda^4}|K_w|^2 Z. \tag{1}$$

This quantity is based on the geometry and statistics of the raindrops (Doviak and Zrnic 1993). The radar wavelength, λ, is 2.24 cm, $|K_w|$ is a function of the refractive index of water, and Z is in mm^6 m^3. Therefore, the same reflectivity factor estimated by the NEXRAD (frequency = 2.9 GHz) can be included in these radar cross-section calculations at the QuikSCAT frequency, if the assumption is made that the effect of Mie scattering is relatively small in this circumstance. To include the effect of attenuation within the volume, the coefficient used was based on the empirical investigations of Iguchi et al. (2000). These functions can then be used to derive a calculation of the NRCS, as a function of Z, which is easily converted to rain rate. The relation we use, $Z = 300R^{1.4}$ is used commonly by NWS, and is a compromise between stratiform and convective rain relationships. It is also within 0.5 dB of the value obtained using one of the Tropical Rainfall Mapping Mission (TRMM) algorithms (Iguchi et al. 2000). This definition allows a comparison of the relative magnitudes of the normalized radar cross section of the sea surface (upon which the scatterometer algorithms are based) and that of the atmospheric rain layer. The latter also requires an assumption of the thickness of the rain layer. Considering the high degree of spatial variability of rain structures, this is a tenuous assumption, but necessary in order to produce numerical estimates. A layer thickness of 4 km was selected. The calculation is based on the integral

$$\sigma_a = \sigma_{vr}\int_0^L e^{-0.461\kappa r}\,dr, \tag{2}$$

where σ_a is the NRCS of a planar (one-dimensional) model, L = 4 km, and κ is the attenuation function of

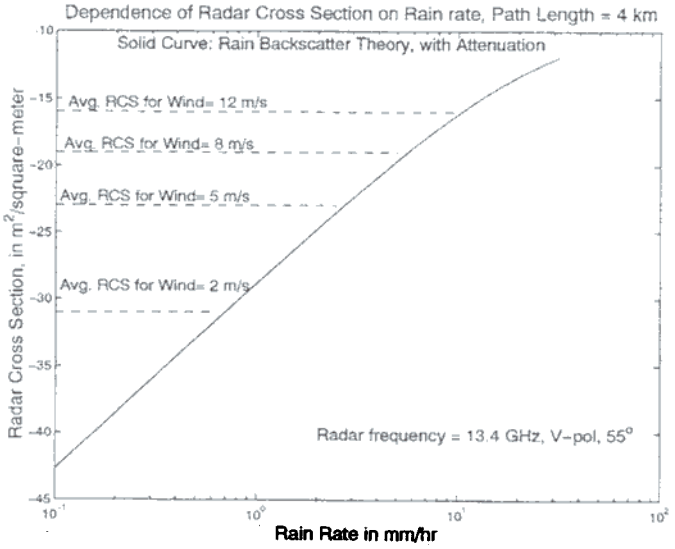

FIG. 7. Computation of the total radar cross section per square meter from an atmospheric layer, 4 km thick, taking into account volumetric backscatter with (and without) attenuation, as a function of rain rate and Z, the radar reflectivity factor ($Z = 300R^{1.4}$). For comparison, the average V-polarized radar cross section of a wind roughened sea, at wind speeds from 2 to 12 m s^{-1} is indicated to note when atmospheric rain will dominate the backscatter signal at the satellite scatterometer. A similar set of lines for H-pol ocean NRCS would be 1–2 dB lower in a radar cross section.

Z, in dB km^{-1}. This distance was selected as a reasonable slant range through the rain layer, not as a possible parameter for the freezing level height. This may be viewed as a simplified but necessary step in modeling the structure of the rain volume, which is highly variable in several dimensions, as seen in Fig. 2.

The results of this calculation can be seen in Fig. 7, in which the solid curve in the graph is based on Z, but the abcissa was converted to rain rate (R). This calculation includes attenuation as indicated in Eq. (2). The azimuthally averaged V-polarized NRCS of the sea surface is also indicated at discrete decibel levels for wind speeds from 2 to 12 m s^{-1}, so they can be compared with the normalized radar cross section of the rain volume. The H-polarized normalized radar cross section of the sea surface (not displayed) is known to be lower by a few decibels, even with a small incidence angle, until the wind speeds approach 20 m s^{-1}. This graph shows that the NRCS will experience a slower rate of increase as the rain rate increases above 10 mm h^{-1}, because attenuation will limit penetration of the radar signal into the volume. The necessary assumption of selecting a layer thickness can be reexamined. If the rain layer thickness is changed from 4 km, these curves will move higher or lower accordingly. These results show that a rain rate close to 2 mm h^{-1} will begin to affect the total radar cross section when surface winds are 5 m s^{-1}, but will not have a discernible effect for surface winds of 12 m s^{-1}. However, a rain rate of 10 mm h^{-1} will affect the scatterometer estimates at this greater wind speed. Again, the thickness of the rain layer will have a direct impact on the scatterometer data.

A significant finding of this analysis is observed when we examine both Figs. 4 and 6 for the wind error values where the rain rate reaches about 15 mm h^{-1}. Despite the different buoy winds of these cases, in each case the scatterometer is estimating the winds to be in the range of 19–23 m s^{-1}. The inference is that at this high a rain rate (and these wind speeds), the scatterometer radar cross section is only influenced by the volumetric backscatter. Referring to the solid curve of Fig. 7 (upper graph), a rain rate of 15 mm h^{-1} will have an NRCS of about −14 dB. This value of NRCS corresponds to what the scatterometer would infer it to be at a wind speed of 20 m s^{-1} (Wentz and Smith 1999). The integral of Eq. (2) indicates that this NRCS will continue to increase with Z, but at a fairly slow rate. These results support the conclusion that, in conditions such as the examples presented here, the volumetric rain backscatter can be the dominant mechanism affecting the radar cross section measured by the scatterometer. In addition, the theoretical model results of Fig. 7 can explain many of the attributes of the measured results of Figs. 4 and 6. The limitations mentioned above regarding the selected Z–R relation should be kept in mind in evaluating Fig. 7 and in considering other choices and conditions.

A comparison of these rain effects can be made to the C-band scatterometer on the European Remote-Sensing Sattelites (*ERS-1/2*). The ratio of the C-band electromagnetic wavelength to that of SeaWinds is approximately 2.5. Applying Eq. (1) to the ERS measurements yields a volumetric backscatter that is 16 dB lower, for a given value of Z. In addition, studies by Tournadre and Morland (1997) have shown that the attenuation coefficient for the ERS frequency is a factor of 13 lower than that of Ku band, at $R = 10$ mm h^{-1}. This factor increases with decreasing values of R. Measurements conducted by *ERS-1* with a tropical cyclone help clarify this issue (Quilfen et al. 1998). Rain measurements in that study were provided by the SSM/I during coincident observations. Their conclusion was that they could find only small and infrequent rain effects on the NRCS, with the exception of the highest rainbands in the storm.

5. Discussion

The size of the errors seen in Fig. 4 makes rain-contaminated scatterometer data unusable in its current form and indicates a more general concern about the usefulness of global datasets in areas of frequent rain. In order for scatterometer data to be useful to the scientific community, it is necessary to identify those areas where rain exists and to gain information about the impact of rain conditions on scatterometer performance. Several empirical studies sponsored by the QuikSCAT science team are in progress to develop insight and skills that will permit the detection of rain conditions directly from the attributes of the received scatterometer signal and associated measurements (Huddleston and Stiles

2000; Mears et al. 2000; Jones et al. 2000). These studies have been incorporated into two different rain-flagging parameters included with the Level 2B data files provided by the Physical Oceanography Distributed Active Archive Center (PO.DAAC) of the Jet Propulsion Laboratory. These rain-flagging scientific datasets provide a quantitative estimate of the likelihood that rain is contaminating the wind estimates (JPL 2001). It is anticipated that the techniques developed in this study can be applied to the evaluation of the effectiveness of these rain flags and to their continued development.

The data analysis and theoretical model presented here combine empirical methods with physical reasoning to identify and separate the several electromagnetic issues that are fundamental to the remediation of the rain problem. The combination of the buoy and NEXRAD rain measurements provides a unique opportunity to systematically develop a collection of data spanning a variety of conditions. This paper is intended to present the early results of this program. These results also demonstrate the success of the methods being applied here. We can see that strongest relative effects take place under the lower wind speed conditions, where moderate rain can become the dominant scattering mechanism. Also suggested by the measurements and the theory is that the scatterometer tends to produce a "maximum" wind speed when the rain dominates because of the physics of rain backscatter and attenuation. This artificial level tends to be in the range of 20–25 m s^{-1}. More observations over a wide range of conditions will guide the physical modeling effort and may lead to techniques that can correct scatterometer measurements and/or determine when rain contamination leads to serious errors.

Acknowledgments. This research was supported by the Physical Oceanography Program of the National Aeronautics and Space Administration through grants to Hofstra University and the Center for Ocean–Atmospheric Prediction Studies, The Florida State University (through support by the JPL QuikSCAT Project). We would also like to acknowledge the support provided by the National Weather Service through a COMET Partners project grant administered by the University Corporation for Atmospheric Research, Boulder, Colorado. We are also grateful to Dr. Larry Bliven of the NASA/Goddard Space Flight Center/Wallops Flight Facility for his assistance, encouragement, and support.

REFERENCES

Battan, L. J., 1973: *Radar Observation of the Atmosphere.* University of Chicago Press, 324 pp.

Bourassa, M. A., M. H. Freilich, D. M. Legler, W. T. Liu, and J. J. O'Brien, 1997: Wind observation from new satellite and research vessels agree. *Eos, Trans. Amer. Geophys. Union,* **78,** 597, 602.

——, D. M. Legler, J. J. O'Brien, and S. R. Smith, 2002: SeaWinds validation with research vessels. *J. Geophys. Res.,* in press.

Craeye, C., 1998: Study of microwave scattering from rain and wind roughened seas. Ph.D. thesis, Universite Catholique de Louvain, Louvain, Belgium, 243 pp.

——, P. W. Sobieski, and L. F. Bliven, 1997: Scattering by artifical wind and rain roughened water surfaces at oblique incidences. *Int. J. Remote Sens.,* **18,** 2241–2246.

Doviak, R. J., and D. S. Zrnic, 1993: *Doppler Radar and Weather Observations.* 2d ed. Academic Press, 562 pp.

Durden, S. L., Z. S. Haddad, A. Kitiyakara, and F. Li, 1998: Effects of nonuniform beam filling on rainfall retrieval for the TRMM precipitation radar. *J. Atmos. Oceanic Technol.,* **15,** 635–646.

Ebuchi, N., 2001: Evaluation of wind vectors observed by QuikSCAT/SeaWinds using ocean buoy data. *Proc. IEEE Int. Geoscience and Remote Sensing Symp.,* Sydney, Australia, IEEE.

Freilich, M. H., and R. S. Dunbar, 1999: The accuracy of the NSCAT-1 vectors: Comparison with National Data Buoy Center buoys. *J. Geophys. Res.,* **104** (C5), 11 231–11 246.

Huddleston, J. N., and B. W. Stiles, 2000: A multidimensional histogram rain-flagging technique for SeaWinds on QuikSCAT. *Proc. IEEE Int. Geoscience and Remote Sensing Symp.,* Vol. 3, Honolulu, HI, IEEE, 1232–1234.

Hunter, S. M., 1996: WSR-88D radar rainfall estimation: Capabilities, limitations and potential improvements. *Natl. Wea. Rev.,* **20,** 26–38.

Iguchi, T., T. Kozu, R. Meneghini, J. Awaki, and K. Okamoto, 2000: Rain profiling algorithm for the TRMM precipitation radar. *J. Appl. Meteor.,* **39,** 2038–2052.

Jones, W. L., M. Susanj, J. Zec, and J. Park, 2000: Validation of QuikSCAT radiometric estimates of rainrate. *Proc. IEEE Int. Geoscience and Remote Sensing Symp.,* Vol. 3, Honolulu, HI, IEEE, 1229–1231.

JPL, 2001: NASA QuikSCAT science data product user's manual: Overview and geophysical data products. Version 2.1. JLP Publ. D-18053, Pasadena, CA, 86 pp.

Klazura, G. E., and D. A. Imy, 1993: A description of the initial set of analysis products available from the NEXRAD WSR-88D system. *Bull. Amer. Meteor. Soc.,* **74,** 1293–1311.

Mears, C. A., D. Smith, and F. J. Wentz, 2000: Detecting rain with QuikSCAT. *Proc. IEEE Int. Geoscience and Remote Sensing Symp.,* Vol. 3, Honolulu, HI, IEEE, 1235–1237.

Moore, R. K., Y. S. Yu, A. K. Fung, D. Kaneko, G. Dome, and R. Werp, 1979: Preliminary study of rain effects on radar scattering from water surfaces. *IEEE J. Oceanic Eng.,* **OE-4,** 31–32.

Portabella, M., and A. Stoffelen, 2001: Rain detection and quality control of SeaWinds. *J. Atmos. Oceanic Technol.,* **18,** 1171–1183.

Quilfen, Y., B. Chapron, T. Elfouhaily, K. Katsaros, and J. Tournadre, 1998: Observation of tropical cyclones by high-resolution scatterometry. *J. Geophys. Res.,* **103** (C4), 7767–7786.

Schumacher, C., and R. A. Houze Jr., 2000: Comparison of radar data from the TRMM satellite and Kwajalein ocean validation site. *J. Appl. Meteor.,* **39,** 2151–2164.

Tournadre, J., and J. C. Morland, 1997: The effects of rain on TOPEX/Poseidon altimeter data. *IEEE Trans. Geosci. Remote Sens.,* **35,** 1117–1135.

Ulaby, F. T., A. Fung, and R. K. Moore, 1981: *Microwave Remote Sensing, Active and Passive.* Vol. 1. Addison-Wesley, 456 pp.

Ulbrich, C. W., and L. G. Lee, 1999: Rainfall measurement error by WSR-88D radars due to variations in Z–R law parameters and the radar constant. *J. Atmos. Oceanic Technol.,* **6,** 1017–1024.

Wentz, F. J., 1997: A well-calibrated ocean algorithm for special sensor microwave/imager. *J. Geophys. Res.,* **102** (C4), 8703–8718.

——, and D. K. Smith, 1999: A model function for the ocean-normalized radar cross section at 14 GHz derived from NSCAT observations. *J. Geophys. Res.,* **104** (C5), 11 499–11 514.